Buckling Behavior of Compression-Loaded Symmetrically Laminated Angle-Ply Plates with Holes

Michael P. Nemeth*
NASA Langley Research Center, Hampton, Virginia

An approximate analysis for buckling of a rectangular specially-orthotropic plate with a central circular hole is applied to symmetrically laminated angle-ply plates. Results obtained from finite-element analyses and experiments indicate that the approximate analysis predicts accurately the buckling loads of $[(\pm\theta)_m]_s$ plates with integer values of $m \geq 6$ and with hole diameters up to 50% of plate width. Moreover, results indicate that the approximate analysis can be used to predict the buckling trends of plates with hole diameters up to 70% of plate width. Results of a parametric study indicate the influence of hole size, plate aspect ratio, loading and boundary conditions, and orthotropy on the buckling load. Results are also presented that indicate the relationship of bending stiffness and the prebuckling load distribution to the buckling load of a plate with a hole.

Nomenclature

d = hole diameter (see Fig. 1)
EA = prebuckling stiffness
D_{11}, D_{22} = bending stiffnesses
K = buckling coefficient
L = plate length (see Fig. 1)
m = stacking sequence number
N_x, N_y, N_{xy} = membrane stress resultants
N_x^o = applied stress loading (see Fig. 1)
N_x^{cr} = value of applied stress loading at buckling
P_{cr} = axial load at buckling
W = plate width (see Fig. 1)
λ = applied edge displacement (see Fig. 1)
θ = fiber orientation angle (see Fig. 1)

Introduction

With the increasing demand for lighter and stronger aircraft structures, the use of advanced composite materials and the search for ways to exploit fully their properties continues. The added degree of freedom of tailoring structural stiffness by altering fiber orientation and stacking sequence provides new structurally efficient design options not offered by metals. A class of composite plates that appears to have potential advantages for use in flight structures is the symmetrically laminated angle-ply plate. This paper examines the buckling behavior of compression-loaded rectangular symmetric angle-ply plates with a central circular hole. This plate configuration serves as an example of a structural component in an aircraft whose behavior is influenced by a local discontinuity.

Intuition may suggest that introducing a large hole into a compression-loaded plate can cause a reduction in the buckling load of the plate. Previous studies of the buckling behavior of isotropic plates with holes, such as the study by Ritchie and Rhoades (Ref. 1), have shown that introducing a hole into a plate does not always reduce the buckling load and, in some instances, may increase its buckling load. This notion was studied further in Ref. 2 for selected specially-orthotropic laminates. Reference 2 shows, both analytically and experimentally, that orthotropy has a significant influence on the buckling load of a plate and that the boundary conditions and loading conditions substantially influence the effect of the hole on the buckling load of a plate.

Changes in orthotropy of symmetrically laminated angle-ply plates can be identified with changes in a single parameter, namely, the fiber orientation angle. These laminates also possess anisotropy in the form of coupling between pure bending and twisting of the midplane of the plate. In Ref. 3 it is shown that the importance of the anisotropy on buckling of rectangular plates without holes diminishes as the number of layers comprising the angle-ply laminate increases. In this paper, the importance of the D_{16} and D_{26} anisotropic constitutive terms is also examined to determine if hole size affects the importance of anisotropy.

The approximate analysis presented in Ref. 2 is used in this paper to obtain buckling loads for angle-ply plates in which anisotropy is negligible. Finite-element results are discussed and experimental results are presented to establish the applicability of the approximate analysis presented in Ref. 2 to symmetrically laminated angle-ply plates with holes. Using the approximate analysis, results of a parametric study are presented that illustrate the influence of orthotropy, hole size, aspect ratio, loading conditions, and boundary conditions on the buckling load. A discussion of how each of these parameters affect the buckling behavior of the plates is presented. The loading conditions considered in this paper are uniform-edge-displacement and uniform-edge-stress loadings. The boundary conditions considered are simply supported conditions on the unloaded edges and either clamped or simply supported conditions on the loaded edges.

Analysis Description

The approximate analysis used in this study of the buckling of rectangular compression-loaded specially-orthotropic plates with centrally located cutouts and uniform thickness is presented in Ref. 2. Loading is applied by either uniformly displacing or uniformly stressing two opposite edges of the plate in the manner shown in Fig. 1. Plates subjected to these two loading cases are sometimes referred to in this paper as dis-

Presented as Paper 86-0922-CP at the AIAA/ASME/ASCE/AHS 27th Structures, Structural Dynamics and Materials Conference, San Antonio, TX, May 19–21, 1986; received Aug. 21, 1986; revision received Sept. 27, 1987.

*Aerospace Engineer, Structural Mechanics Branch, Structures and Dynamics Division.

placement-loaded and stress-loaded plates. The boundary conditions used in the analysis are simply supported conditions on the unloaded edges and either clamped or simply supported conditions on the loaded edges. The plates are allowed to deform freely in-plane in the transverse direction at the unloaded edges. The classical two-dimensional analysis for determining the plate buckling load is converted to an approximately equivalent one-dimensional analysis. This conversion is carried out by expressing the plate displacements as series with each element containing a trigonometric function of one coordinate and a coefficient that is an arbitrary function of the other coordinate. Ordinary differential equations with variable coefficients are derived by applying a variational principle.

Experiment

The specimens tested in this investigation were fabricated from commercially available 450 K (350°F) cure graphite-epoxy preimpregnated tapes. The tapes were made of unidirectional Hercules AS4 graphite fibers preimpregnated with Hercules 3502 thermosetting epoxy resin. Nominal lamina properties were assumed to include a longitudinal modulus $E_1 = 127.8$ GPa (18.5×10^6 psi), a transverse modulus $E_2 = 11.0$ GPa (1.6×10^6 psi), and in-plane shear modulus $G_{12} = 5.7$ GPa (0.832×10^6 psi), a major Poisson's ratio $\nu_{12} = 0.35$, and a nominal thickness of 0.127 mm (0.005 in.). The tapes were laid up to form 24-ply-thick laminates having $[(\pm 60)_6]_s$ stacking sequences. The laminates were cured in an autoclave using the manufacturer's recommended procedures. After curing, the laminates were ultrasonically C-scanned to assess specimen quality and then machined into test specimens.

All specimens were 25.4 cm (10 in.) long by 25.4 cm (10 in.) wide and the loaded edges were machined flat and parallel to permit uniform compressive loading. Central circular holes were machined into the panels using diamond impregnated core drills. The hole diameters ranged from 0 to 15.96 cm (6.28 in.). One side of each specimen was painted white to reflect light so that a moire-fringe technique could be used to monitor the out-of-plane deformations. The specimens were loaded in axial compression using a 0.51-MN (300-kip)-capacity hydraulic testing machine. The loaded ends of the specimens were clamped by fixtures during testing and the sides were simply supported by restraints that prevent the specimen from buckling as a wide column. All specimens were loaded slowly to approximately twice the buckling load. A typical specimen mounted in the test fixture is shown in Fig. 2. A total of nine specimens, designated as specimen A1–A5 for the $[(\pm 30)_6]_s$ specimens and B1–B4 for the $[(\pm 60)_6]_s$ specimens, were tested.

Electrical resistance strain gages were used to measure strains, and direct-current differential transformers were used to measure axial displacements and displacements normal to the specimen surface. Electrical signals from the instrumentation and the corresponding applied loads were recorded on magnetic tape at regular time intervals during the tests.

Results and Discussion

Importance of Anisotropy

Symmetrically laminated composite plates display anisotropy in the form of a material-induced coupling between pure bending and twisting of the plate midplane due to the presence of the D_{16} and D_{26} constitutive terms. It was shown in Ref. 3 that neglecting these terms in a buckling analysis of a rectangular plate without a hole does not appreciably affect the buckling predictions for $[(\pm\theta)_m]_s$ laminates having integer values of $m \geq 6$.

To determine the effect of hole size on the importance of anisotropy, finite-element analyses were conducted using the computer program known as EAL.[4] A mesh refinement study was performed to obtain an estimate of the accuracy of the finite-element analyses. Using Ref. 3 as a guide, buckling coefficients were obtained for $[(\pm 60)_6]_s$ and $[(\pm 60)_6/(-60)_6]_s$ displacement-loaded angle-ply plates with ratios of hole diameter to plate width d/W ranging from zero to 0.6.

The nondimensional buckling coefficient is given by

$$K = \frac{N_x^{cr} W^2}{\pi^2 \sqrt{D_{11} D_{22}}} \tag{1}$$

where W is the plate width and D_{11} and D_{22} are bending stiffnesses. For the stress-loaded plates, N_x^{cr} is the critical value of the applied loading N_x^o. For the displacement-loaded plates, N_x^{cr} is obtained by dividing the total axial load at buckling P_{cr} by the plate width. References 3 suggests that the $[(\pm 60)_6]s$ laminates behave like specially-orthotropic plates. Similarly, the $[(+60)_6/(-60)_6]_s$ laminates do not behave like specially-orthotropic laminates. This assessment is based on values of 0.08 and 0.50 for the largest of the anisotropic parameters (see Ref. 3) corresponding to the $[(\pm 60)_6]_s$ and $[(+60)_6/(-60)_6]_s$ laminates, respectively.

The results obtained for these laminates indicated that the effect of anisotropy on the buckling loads is the same for hole sizes up to $d/W = 0.3$. Beyond $d/W = 0.3$, interaction between hole size and anisotropy occurs. The results obtained for these laminates also indicated increases in the differences between buckling coefficients, due to anisotropy, of at most 2% for $d/W \leq 0.3$, 4% for $d/W = 0.4$, 7% for $d/W = 0.5$, and 12% for $d/W = 0.6$ as compared to the difference in buckling co-

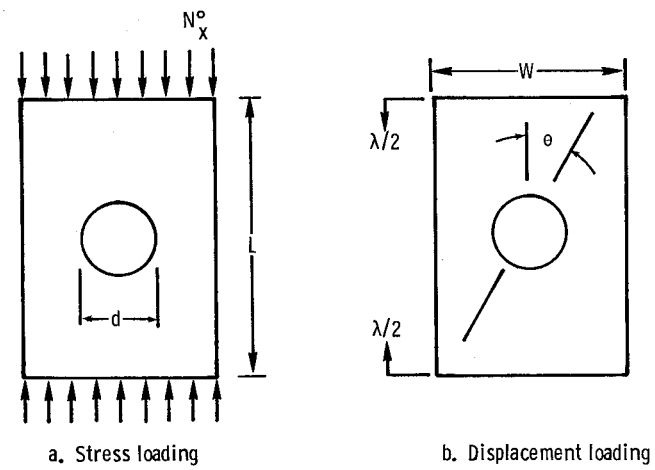

Fig. 1 Plate geometry and loading conditions.

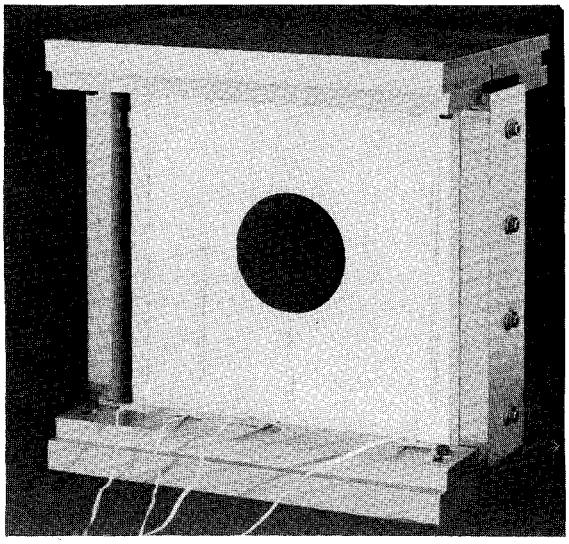

Fig. 2 Specimen mounted in test fixture.

efficients for $d/W = 0.0$. A finite-element analysis for a $[(\pm 60)_{12}]_s$ plate with $d/W = 0.6$ produced a buckling coefficient that was less than 1% different from the buckling coefficient of the $[(\pm 60)_6]_s$ plate with $d/W = 0.6$. This result suggests that the anisotropy is negligible in the $[(\pm 60)_6]_s$ plates with holes. The results previously discussed suggest that increasing hole size increases the importance of anisotropy in the $[(+60)_6/(-60)_6]_s$ plates. Neglecting the anisotropy in the analysis of one of these plates with $d/W = 0.6$ results in a buckling coefficient that is 37% too large compared to 24% too large for the same plates with $d/W = 0$.

Comparison with Finite-Element and Experimental Results

Buckling loads calculated by the approximate analysis for angle-ply laminates with 24 or more plies were compared with buckling loads obtained from EAL. Results for simply supported square $[(\pm 60)_m]_s$ laminates ($m \geq 6$), loaded by uniform edge displacement, were investigated first. Hole diameters ranging in size from zero to 60% of the plate width were considered.

Good agreement between the results obtained using the approximate analysis and the finite-element analysis was found. The largest difference in the results obtained using the two analysis methods was about 10% for $d/W = 0.6$. Similar results were obtained for corresponding simply supported plates subjected to uniform-edge-stress loading, and clamped plates subjected to uniform-edge-displacement loading.

The approximate analysis results and experimental results are compared in Fig. 3 and in Tables 1 and 2. The analytical results presented in Fig. 3 and in Tables 1 and 2 are based on length and width dimensions of 24.13 cm (9.50 in.). These dimensions represent the portion of the plate between edge supports of the test fixture (see Fig. 2) that deforms out-of-plane when buckling occurs. The analytical results are also based on the average value of several thickness measurements made on each specimen. The average value was determined to be 2.9870 mm (0.1176 in.) for the $[(\pm 30)_6]_s$ and $[(\pm 60)_6]_s$ laminates. The experimental data collected during these tests indicated sharp changes in the slopes of the load-shortening curves at buckling and elastic behavior. The experimental buckling loads for these plates were obtained by extrapolating the prebuckling and postbuckling branches of the load-shortening curves for each case linearly. The intersection of the two straight line extrapolations was taken as the buckling load.

The buckling loads presented in Tables 1 and 2 indicate agreement to within 5% between theory and experiment for the plates with $d/W = 0$, 0.105, and 0.316. The difference in the analysis and experiment for the $[(\pm 30)_6]_s$ plates with $d/W = 0.6$ and 0.66 were approximately 33% and in excess of 80%, respectively. The difference in the analysis and experiment for the $[(\pm 60)_6]_s$ plate with $d/W = 0.66$ was within 25%. Moreover, the approximate analysis predicted the buckling mode shapes of each experiment. The mode shape of all test specimens was one half-wave along each coordinate direction. The best agreement between theory and experiment was exhibited by the $[(\pm 60)_6]_s$ plates. Both laminate types exhibited a trend of increasing buckling load when d/W became larger than 0.32.

The experimental and analytical average buckling strains P_{cr}/EA are shown in Fig. 3. The agreement between theory and experiment is a few percent less than the agreement of the results presented in Tables 1 and 2. The difference in agreement

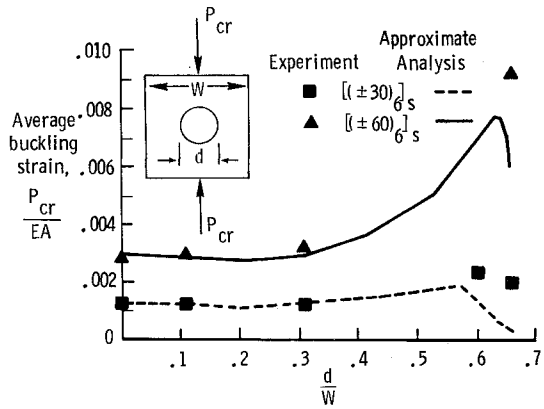

Fig. 3 Experimental and approxiamate average buckling strains for displacement-loaded clamped $[(\pm 30)_6]_s$ and $[(\pm 60)_6]_s$ plates.

Table 1 Experimental and analytical buckling loads for clamped $[(\pm 30)_6]_s$ laminates

Specimen	d/W	Hole diameter cm (in.)	Buckling loads, kN (lb) Experiment	Analysis	Difference[a] percent
A1	0.	0. (0.)	42.894 (9643)	43.975 (9886)	−2.5
A2	.105	2.54 (1.0)	40.510 (9107)	42.040 (9451)	−3.8
A3	.316	7.62 (3.0)	37.668 (8468)	37.783 (8494)	−0.3
A4	.600	14.48 (5.70)	38.686 (8697)	25.947 (5833)	32.9
A5	.660	15.88 (6.25)	38.922 (8750)	5.204 (1170)	86.6

[a]Difference between analysis and experiment.

Table 2 Experimental and analytical buckling loads for clamped $[(\pm 60)_6]_s$

Specimen	d/W	Hole diameter cm (in.)	Buckling loads, kN (lb) Experiment	Analysis	Difference[a] percent
B1	0.	0. (0.)	25.947 (5833)	26.423 (5940)	−1.8
B2	.105	2.54 (1.0)	24.465 (5500)	25.555 (5745)	−4.5
B3	.316	7.62 (3.0)	22.005 (4947)	22.788 (5123)	−3.6
B4	.660	15.88 (6.25)	31.138 (7000)	23.700 (5328)	23.9

[a]Difference between analysis and experiment.

is due to the additional approximation introduced in calculating the prebuckling stiffness. That is, the prebuckling stiffness of the experiments is based on the true length of the plates. The prebuckling stiffness of the analysis is based on the unsupported length between the clamped edges previously discussed. The results in Fig. 3 suggest that the approximate analysis for the clamped plates becomes deficient when $d/W > 0.56$ for the $[(\pm 30)]_s$ plates and $d/W > 0.63$ for the $[(\pm 60)_6]_s$ plates. However, by plotting the approximate analysis results for $0 \le d/W \le 0.7$, the trend in the buckling behavior and the expected deficiency in the analysis can be easily identified.

As the hole gets larger, a point is approached at which the plate's buckling resistance drops off dramatically. This point corresponds to local buckling of one or more of the plate ligaments between the hole and lateral supports. The analysis for both the $[(\pm 30)_6]_s$ and $[(\pm 60)_6]_s$ laminates, and the experimental results for the $[(\pm 30)_6]_s$ laminates presented in Fig. 5 indicate this trend. The analysis typically indicates the drop-off in buckling strain to occur at a d/W slightly smaller than that of the corresponding experiments. Moreover, the drop-off in buckling strain for the $[(\pm 30)_6]_s$ laminates occurs at a substantially smaller d/W and with much less severity than the drop-off exhibited by the $[(\pm 60)_6]_s$ laminates. This difference in prediction between experiment and analysis at which the buckling strain drop-off occurs accounts for the large differences in buckling loads and strain for $d/W \ge 0.6$ previously mentioned.

Parametric Study

The results of the parametric study presented in this paper were obtained using the approximate analysis presented in Ref. 2. Results that indicate the buckling coefficient K as a function of d/W and the fiber orientation angle θ for square $[(\pm\theta)_m]_s$ laminates with integer values of $m \ge 6$ are shown in Figs. 4–7 for values of $0 \le d/W \le 0.6$. The results shown in Figs. 4 and 5 are for simply supported plates subjected to uniform-edge-displacement and uniform-edge-stress loadings, respectively. The results shown in Figs. 6 and 7 are for clamped plates subjected to uniform-edge-displacement and uniform-edge-stress loadings, respectively. Results that indicate the buckling coefficient K as a function of aspect ratio L/W, boundary conditions, and loading conditions are shown in Fig. 8. The results presented in Fig. 8 are for $[(\pm 15)_m]_s$ plates ($m \ge 6$), with $d/W = 0.0$ and 0.4. Similar results for $[(\pm 45)_m]_s$ and $[(\pm 75)_m]_s$ plates were presented by the author in Ref. 5 and are discussed herein.

Results for Square Plates

The results shown in Fig. 4 for the displacement-loaded simply supported plates indicate that the plates with $\theta = 90$ deg and $\theta = 45$ deg have the lowest and highest buckling coefficients, respectively, for the full range of d/W. Moreover, the results illustrated in this figure indicate that the plates exhibit an increase in buckling coefficients with increasing d/W to some extent. The results shown in Fig. 5 for the stress-loaded simply supported plates exhibit, for the most part, different trends in the buckling behavior than the displacement-loaded plates. With the exception of the plates with $\theta \ge 45$ deg, the stress-loaded plate results illustrated in Fig. 5 typically exhibit more of a monotonic reduction in buckling load with increasing d/W than do the displacement-loaded plates illustrated in Fig. 4. The results shown in Figs. 6 and 7 for the displacement-loaded and stress-loaded clamped plates, respectively, indicate that the clamped plates exhibit altogether different trends in buckling behavior than the simply supported plates. Displacement-loaded clamped plates with $\theta = 90$ and 75 deg exhibit reductions in buckling load followed by increases in buckling load as d/W increases, unlike the simply supported plates.

Results for Rectangular Plates

Results for rectangular plates with $d/W = 0.0$ and 0.4 and with $\theta = 15$ deg are presented in Fig. 8. The results shown in Fig. 8 for the clamped and simply supported plates with $d/W = 0.4$ indicate that the differences in buckling load due to the differences in loading conditions attenuate to values within 5% of one another at $L/W = 2.0$ and to values within 1% of one another at $L/W = 3.4$. The results of Fig. 8 also indicate that the differences in buckling load due to the difference in

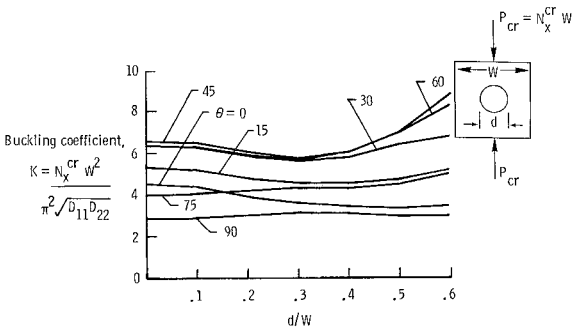

Fig. 4 Buckling coefficients for displacement-loaded simply supported $[(\pm\theta)_m]_s$ ($m \ge 6$) square plates.

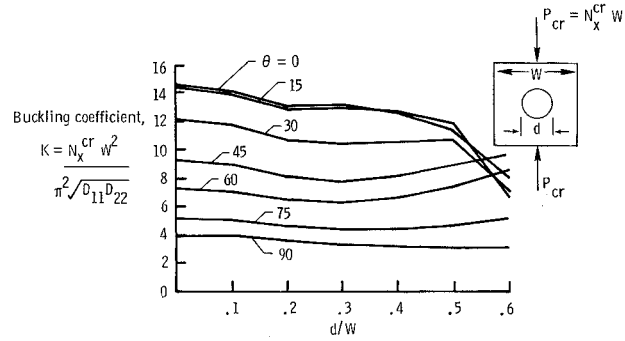

Fig. 6 Buckling coefficients for displacement-loaded clamped $[(\pm\theta)_m]_s$ ($m \ge 6$) square plates.

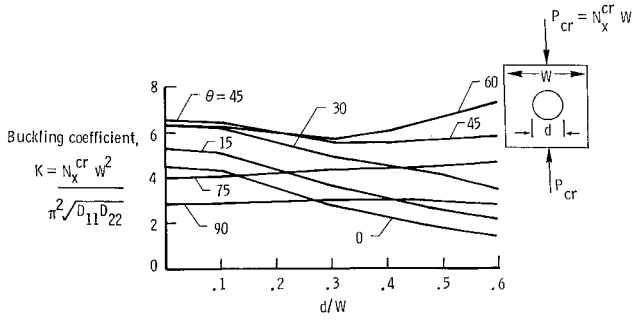

Fig. 5 Buckling coefficients for stress-loaded simply supported $[(\pm\theta)_m]_s$ ($m \ge 6$) square plates.

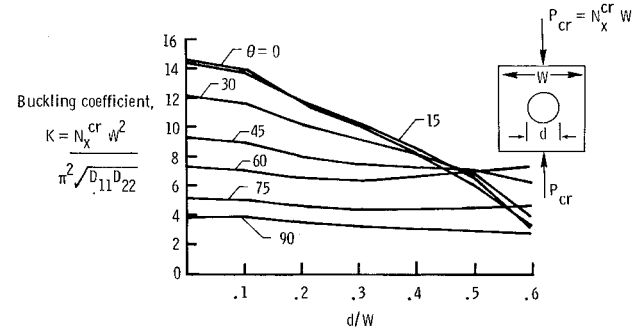

Fig. 7 Buckling coefficients for stress-loaded clamped $[(\pm\theta)_m]_s$ ($m \ge 6$) square plates.

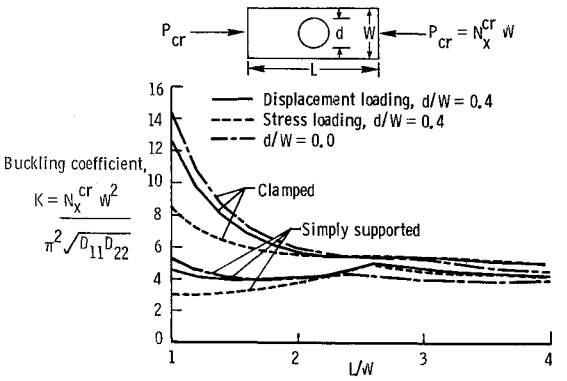

Fig. 8 Buckling coefficients for displacement-loaded and stress-loaded clamped and simply supported $[(\pm 15)_m]_s$ ($m \geq 6$) rectangular plates ($d/W = 0.0$ and 0.4).

boundary conditions attenuate to values within 13% of one another for the plates with $d/W = 0.0$ at $L/W = 4$, and attenuate to values within 18% of one another for the plates with $d/W = 0.4$ at $L/W = 4$.

Results for rectangular plates with $d/W = 0.0$ and 0.4 and with $\theta = 45$ deg (see Ref. 5) indicate that differences in buckling load due to the differences in loading conditions for the clamped and simply supported plates with holes attenuate to values within 1% of one another at $L/W = 1.2$ and to values within 0.5% at $L/W = 2.8$. Moreover, these results indicate that the differences in buckling load due to the difference in boundary conditions attenuate to values within 10% of one another at $L/W = 2.2$ for the plates with $d/W = 0.0$ and at $L/W = 1.4$ for the plates with $d/W = 0.4$. Attenuation in the buckling loads to values within 1% of one another occurs at $L/W = 3.6$ for the plates with $d/W = 0.4$ and to within 4% at $L/W = 3.4$ for the plates with $d/W = 0.0$.

Results for the rectangular plates with $d/W = 0.0$ and 0.4 and with $\theta = 75$ deg (see Ref. 5) indicate that differences in buckling load due to the differences in loading conditions of the clamped and simply supported plates with $d/W = 0.4$ are within 1% of one another for $L/W = 1$ and attenuate to values less than 1% of one another at $L/W = 1.2$.

The results of Fig. 8 and the corresponding results presented in Ref. 5 indicate that the differences in buckling load due to the difference in boundary conditions and loading conditions attenuate the fastest for the plates with $\theta = 75$ deg followed by the plates with $\theta = 45$ and 15 deg, respectively. Moreover, the differences in buckling load due to difference in boundary conditions for the plates with $\theta = 45$ and 75 deg and with $d/W = 0.0$ attenuate at higher plate aspect ratios than the same plates with $d/W = 0.4$. The plates with $\theta = 15$ deg exhibit the opposite trend. The differences in buckling load due to difference in boundary conditions attenuate substantially slower than the difference in buckling load due to difference in loading conditions. The results shown in Fig. 8 and presented in Ref. 5 also suggest that the highest attenuation rate is exhibited by the plates with $\theta = 90$ deg and the slowest rate by the plates with $\theta = 0$. The aspect ratio at which differences in buckling loads due to differences in loading conditions attenuate is expected to decrease as d/W decreases. The aspect ratio at which differences in buckling loads due to differences in boundary conditions attenuate is expected to decrease as d/W increases.

Discussion of the Buckling Behavior

Results presented in this paper indicate that increasing the hole size in a plate can in some cases result in increasing the buckling load of the plate. It has been suggested in Refs. 6 and 7 that the buckling load of a plate with a hole depends on the reduction in bending stiffness due to the hole, and the influence of the prebuckling load distribution in the plate. This stiffness reduction makes the plate more susceptible to buckling when the axial in-plane load path acts closer to the hole edges than to the unloaded edges of the plate. The extent to which the bending stiffness is reduced and the prebuckling load path is distributed around the hole depends upon hole size, boundary and loading conditions, plate aspect ratio, and orthotropy of the plate. An analysis in which only the reduction in bending stiffness is included in computing the buckling load would show a monotonic decrease in the buckling load as d/W increases. The effect of the prebuckling load distribution is to either amplify the rate of reduction in buckling load with increasing d/W or to act in an opposite manner depending on in-plane boundary conditions, loading conditions, and orthotropy. Results that show a monotonic reduction in the ordinate with increasing d/W characterize a plate as being dominated by the loss in bending stiffness that occurs as the hole size increases. Results that show increases in the ordinate as d/W increases are associated with the prebuckling load distribution as the source of increases in buckling load.

Behavior of Square Plates

The results for the displacement-loaded simply supported plates shown in Fig. 4 indicate that the plates with fiber orientations closest to 0 deg exhibit the larger reductions in buckling load with increasing d/W. The plates with fiber orientations closest to 90 deg exhibit very little reduction in buckling load with increasing d/W and in some cases no reduction in buckling load. The increases in buckling load shown in Fig. 4 suggest that the axial prebuckling load path in the plates with $\theta = 45$ and 60 deg shifts away from the hole as d/W increases. Larger increases in buckling load are expected as the load path shifts farther away from the hole.

Results for the simply supported stress-loaded plates shown in Fig. 5 suggest that the prebuckling load distribution for the stress-loaded plates is typically different than for the displacement-loaded plates. The results in Fig. 5 show a monotonic reduction in buckling load with increasing d/W for the plates with $\theta \leq 30$ deg. This trend suggests that the axial prebuckling load path acts closer to the hole edges than to the unloaded edges of the plates. The reduction in bending stiffness due to the hole and location of the in-plane load path result in reducing the buckling load as d/W increases. The results for the plates with $45 \leq \theta \leq 75$ deg suggest that the prebuckling load path acts closer to the unloaded edges of the plate, thus increasing the buckling load. The curve shown in Fig. 5 for the plates with $\theta = 90$ deg indicates an increase in the buckling load as d/W increases to approximately 0.4 and then indicates a decrease in buckling load as d/W increases beyond 0.4. These results suggest that for d/W approximately equal to 0.4 the reduction in bending stiffness contributes more to the buckling behavior than the prebuckling load distribution.

The results shown in Figs. 4–7 suggest that the influence of the bending stiffness on the buckling behavior is in most cases amplified by clamping the loaded edges of the plates. Applying clamped boundary conditions on the loaded edges as opposed to applying simply supported boundary conditions on the loaded edges results in larger reductions in buckling coefficient, as compared to the corresponding plate without a hole, for all the plates with $\theta \geq 30$ deg and for $0 \leq d/W \leq 0.6$. Clamping the loaded edges of the plates with $\theta = 0$ deg causes a similar reduction in buckling coefficient when $d/W \leq 0.1$ and when $d/W = 0.6$. Clamping the loaded edges of the plates with $\theta = 15$ deg similarly causes a reduction in buckling coefficient when $d/W \leq 0.2$ and when $d/W \geq 0.5$.

Contour plots of the prebuckling stress resultants obtained using the approximate analysis for $[(\pm 30)_6]_s$ and $[(\pm 60)_6]_s$ displacement-loaded and stress-loaded plates with $d/W = 0.5$ are presented in Figs. 9 and 10 for the upper left-hand quadrant of the plates. The axial N_x stress resultant contours for both fiber orientations and loading conditions are shown in Fig. 9, and the transverse N_y stress resultant contours are shown in Fig. 10. The stress resultant contours shown in these figures are normalized so they can be compared directly with a uniform value

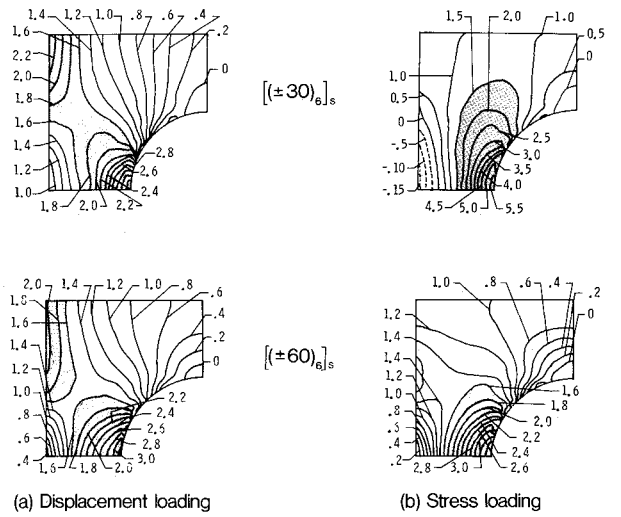

Fig. 9 Contour plots of the normalized prebuckling N_x stress resultant for square $[(\pm 30)_6]_s$ and $[(\pm 60)_6]_s$ plates with $d/W = 0.5$.

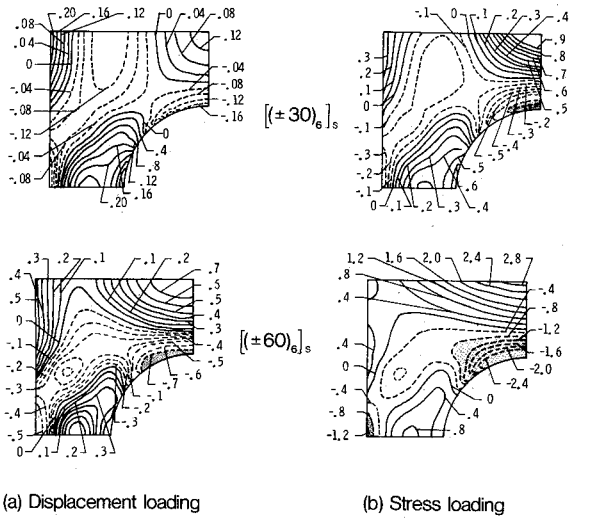

Fig. 10 Contour plots of the normalized prebuckling N_x stress resultant for square $[(\pm 30)_6]s$ and $[(\pm 60)_6]_s$ plates with $d/W = 0.5$.

of one corresponding to the prebuckling stress distribution in the corresponding plate with $d/W = 0$. The stress resultants for the stress-loaded plates with $d/W = 0.5$ were divided by the value of the axial stress resultant in the corresponding plates with $d/W = 0$ for the same magnitude of axial load. The stress resultants for the displacement-loaded plates were divided by the same factor as the stress-loaded plates and then multiplied by the ratio of the axial load in the corresponding stress-loaded plate with $d/W = 0$ to the axial load in the corresponding displacement-loaded plate with $d/W = 0.5$. This multiplication is needed because the displacement-loaded plates with $d/W = 0.0$ and 0.5 have different axial loads for the same applied axial displacement. The regions between contours with values greater than or equal to 1.5 for the N_x stress resultants, and with values less than or equal to -0.7 for the N_y stress resultants, are shaded to indicate the regions of the plate where the loading is most pronounced.

The contour plot of the normalized values of the axial stress resultant N_x for the displacement-loaded $[(\pm 30)_6]_s$ plates indicates that the axial load in these plates acts away from the hole and acts closer to the unloaded edges of the plate as shown in Fig. 9. For the same plate subjected to stress loading, the load acts closer to the central region of the plate where the bending stiffness is lower. The difference in the buckling loads corresponding to these two loading conditions is attributed to the difference in how their axial prebuckling load paths are distributed around the hole. The displacement-loaded plate with the load acting farthest from the hole has the higher buckling load. The results shown in Fig. 9 for the $[(\pm 60)_6]_s$ plates indicate that the axial load acts in essentially the same manner for both loading conditions. This similarity accounts for the similarity of the buckling load curves shown in Figs. 4–7 for the plates with $\theta = 60$ deg. The results for both the displacement-loaded and stress-loaded $[(\pm 60)_6]_s$ plates show that the buckling load increases as d/W increases. This trend is attributed to the fact that the axial prebuckling load path is located outboard of the hole nearer to the unloaded edges of the plates.

The contour plots shown in Fig. 10 suggest that the transverse stress resultant N_y also affects the buckling load of the plate. The effect of the transverse stresses is to develop zones of tensile stresses near the central region of the plate that tend to stabilize the plate in the same manner as applying a transverse tension force to an axially compression-loaded plate. The tensile zones shown in Fig. 10 for the displacement-loaded and stress-loaded $[(\pm 30)_6]_s$ plates are present but have magnitudes much smaller than the order of the magnitudes of the axial stress contours and as a result are expected to be negligible. However, the tensile zones shown in Fig. 10 for the displacement-loaded and stress-loaded $[(\pm 60)_6]_s$ plates have magnitudes of the same order as the magnitudes of the corresponding N_x stress resultant and are expected to contribute to increasing the buckling load. The tensile zone shown in Fig. 10 for the displacement-loaded $[(\pm 60)_6]_s$ plate is located at the top edge of the cutout and has a maximum value of -1.0. The corresponding tensile zone shown in Fig. 10 for the stress-loaded $[(\pm 60)_6]_s$ plate is much larger than the tensile zone in the corresponding displacement-loaded plate and has a maximum magnitude of -2.4.

Behavior of Rectangular Plates

The buckling load of a rectangular plate without a hole is influenced by the aspect ratio of the buckles forming the mode shape. The aspect ratio of the buckles of a corresponding infinitely long plate represents a measure of the plate's natural stability configuration that is independent of the boundary conditions at infinity. For plates with finite length, the aspect ratio of the buckles is influenced by the plate aspect ratio and boundary conditions on the loaded edges. For example, when the plate aspect ratio is a multiple of the aspect ratio of the buckles for the corresponding infinitely long plate, the aspect ratio of the buckles in the finite plate is the same as the aspect ratio of the buckles in the infinitely long plate. Thus, both cases have the same buckling load. When the plate aspect ratio is not a multiple of the aspect ratio of the buckles in the corresponding infinitely long plate, the plate seeks stability of equilibrium at a buckling load higher than the buckling load of the infinitely long plate. The point to be made is that the difference in buckling load is a consequence of a change in aspect ratio of the buckles forming the mode shape that is caused by a change in geometry or boundary conditions.

When a hole is introduced into a rectangular plate, the buckling load is influenced by the loss in bending stiffness and prebuckling load redistribution associated with the hole, in addition to plate aspect ratio effects previously discussed. The hole influences the aspect ratio of the buckles forming the mode shape in a manner similar to the way the loaded-edge boundary conditions influence the aspect ratio of the buckles forming the mode shape of a plate without a hole. For example, changing the loaded-edge boundary conditions from simply supported to clamped suppresses the rotation of the loaded edges of the plate. This restraint acts to change the aspect ratio of the buckles forming the mode shape. Similarly, introducing a hole into a plate can change the buckle pattern from two

half-waves along the length of the plate to a single half-wave along the length. The influence of the hole on the aspect ratio of the buckles forming the mode shape diminishes as the aspect ratio increases because the number of multiples of the buckles corresponding to the infinitely long plate increases to become the dominant factor in the behavior.

The attenuation in the differences in buckling load due to differences in the loading conditions with respect to increasing the aspect ratio of the plate is related to the in-plane deformation state of the plate. The loaded edges of a square displacement-loaded plate deform uniformly in the axial direction to produce a nonuniform axial stress distribution across these edges. The loaded edges of the stress-loaded plate, however, deform nonuniformly across the width. As the aspect ratio of the plate is increased, the deformation states of the two loading conditions coalesce and both loading cases have the same buckling load. The common deformation state is one that is intermediate to the deformation states for the uniform-edge-stress and uniform-edge-displacement loadings. As the aspect ratio increases towards infinity, the stress state in the plate is predominantly uniform axial compression and, hence, the nonuniformity in the prebuckling stress field due to the hole is not expected to substantially influence the buckling behavior of the plate.

Concluding Remarks

An approximate analysis for buckling of a rectangular specially-orthotropic plate with a centrally located cutout has been applied to symmetrically laminated angle-ply plates. Results obtained using finite-element analyses and experimental results suggest that the approximate analysis accurately predicts buckling loads of $[(\pm\theta)_m]_s$ plates with integer values of $m \geq 6$ for $d/W \leq 0.56$ and can be used to predict the general trends for the larger hole sizes. Both analysis and experimental results have been presented that show a trend of increasing buckling load with increasing hole size. Results of a parametric study indicate the influence of hole size, plate aspect ratio, loading conditions, boundary conditions, and orthotropy on a buckling load.

The parametric results presented in this paper indicate that orthotropy, geometry, loading conditions, and boundary conditions play a significant role on the influence of the hole on buckling behavior. Specifically, results are presented that suggest the buckling behavior of square plates depends on the loss in bending stiffness and prebuckling stress distribution associated with the hole. For some fiber orientations and stacking sequences results suggest that the loss in bending stiffness has a more dominant influence on the buckling behavior than the prebuckling stress distribution. Results for clamped and simply supported square plates in which the axial prebuckling load path is located away from the hole suggest that the loss in bending stiffness is less important than for plates in which the axial prebuckling load path is located near the hole. The buckling load increases when the axial prebuckling load path is located away from the hole, and sometimes, even beyond the buckling load for the corresponding plate without a hole. Results for some of the clamped plates are presented that indicate that the loss in bending stiffness plays a more dominant role on the buckling behavior than the prebuckling stress distribution than for simply supported plates. The importance of increases in the loss in bending stiffness on the buckling behavior is associated with reduction in buckling load.

Results presented for rectangular plates with holes indicate that the buckling load depends upon the prebuckling stress distribution and the loss in bending stiffness associated with the different aspect ratio of the buckles. Results are presented that suggest that the effect of the hole diminishes as the plate aspect ratio becomes large. Results are also presented that indicate that the differences in buckling load due to differences in loading conditions attenuate faster in the $[(\pm\theta)_m]_s$ plates as θ approaches 90 deg. Similar trends are shown with respect to the boundary conditions on the loaded edges. The attenuation rates for the loading conditions are shown to be typically faster than for the boundary conditions.

References

[1]Ritchie, D. and Rhoades, J., "Buckling and Postbuckling Behavior of Plates with Holes," *Aeronautical Quarterly*, Vol. 26, Nov. 1975, pp. 281–296.

[2]Nemeth, M. P., Stein, M., and Johnson, E. R., "An Approximate Buckling Analysis for Rectangular Orthotropic Plates With Centrally Located Cutouts," NASA TP-2528, Dec. 1985.

[3]Nemeth, M. P., "Importance of Anisotropy on Buckling of Compression-Loaded Symmetric Composite Plates," *AIAA Journal*, Vol. 24, Nov. 1986, pp. 1831–1835.

[4]Whetstone, W. D., "EAL Engineering Analysis Language Reference Manual," Engineering Information Systems, Inc., Saratoga, CA, Jan. 1979.

[5]Nemeth, M. P., "Buckling Behavior of Compression-Loaded Symmetrically-Laminated Angle-Ply Plates With Holes," AIAA/ASME/ASCE/AHS 27th Structures, Structural Dynamics, and Material Conf., AIAA Paper 86-0922-CP, San Antonio, TX, May 1986.

[6]Kawai, T. and Ohtsubo, H., "A Method of Solution for the Complicated Buckling Problems of Elastic Plates with Combined Use of Rayleigh-Ritz's Procedure in the Finite Element Method," *Proceedings of the Second Conference on Matrix Methods in Structural Mechanics*, AFFDL-TR-68-150, 1968, pp. 967–994.

[7]Vann, W. P. and Vos, R. G., "Compression Buckling of Pierced Elastic Plates," *Structural Research at Rice*, Rept. No. 14, Dept. of Civil Engineering, Rice Univ., Houston, TX, Aug. 1972.